

The Control of the Controller: Molecular Mechanisms for Robust Perfect Adaptation and Temperature Compensation

Xiao Yu Ni,[†] Tormod Drengstig,[‡] and Peter Ruoff^{†*}

[†]Centre for Organelle Research and [‡]Department of Electrical Engineering and Computer Science, University of Stavanger, Stavanger, Norway

ABSTRACT Organisms have the property to adapt to a changing environment and keep certain components within a cell regulated at the same level (homeostasis). “Perfect adaptation” describes an organism’s response to an external stepwise perturbation by regulating some of its variables/components precisely to their original preperturbation values. Numerous examples of perfect adaptation/homeostasis have been found, as for example, in bacterial chemotaxis, photoreceptor responses, MAP kinase activities, or in metal-ion homeostasis. Two concepts have evolved to explain how perfect adaptation may be understood: In one approach (robust perfect adaptation), the adaptation is a network property, which is mostly, but not entirely, independent of rate constant values; in the other approach (nonrobust perfect adaptation), a fine-tuning of rate constant values is needed. Here we identify two classes of robust molecular homeostatic mechanisms, which compensate for environmental variations in a controlled variable’s inflow or outflow fluxes, and allow for the presence of robust temperature compensation. These two classes of homeostatic mechanisms arise due to the fact that concentrations must have positive values. We show that the concept of integral control (or integral feedback), which leads to robust homeostasis, is associated with a control species that has to work under zero-order flux conditions and does not necessarily require the presence of a physico-chemical feedback structure. There are interesting links between the two identified classes of homeostatic mechanisms and molecular mechanisms found in mammalian iron and calcium homeostasis, indicating that homeostatic mechanisms may underlie similar molecular control structures.

INTRODUCTION

Many physiologically important compounds are under tight homeostatic regulation, where internal concentrations are adapted (1) at certain levels, despite environmental disturbances. Two concepts have developed to understand homeostasis: one is related to the intrinsic properties of the network showing that the adaptation response is independent of (most but not all) rate constant values (referred to here as robust (2–4) adaptation/homeostasis), whereas the other concept looks at the homeostasis due to a fine-tuning between rate constants. Perfect adaptation describes an organism’s response to an external stepwise perturbation by regulating some of its variables/components precisely to their original preperturbation values. Perfect adaptation has been found, for example, in bacterial chemotaxis (5–8), photoreceptor responses (9), and MAP-kinase regulation (10–12). In this respect, perfect adaptation and homeostasis are closely related and in the following, we look at homeostasis as a perfectly adapted process.

Robust perfect adaptation/homeostasis of a perturbed system can be related to the concept of integral control (13) or integral feedback (14). In this type of control mechanism, the error between the value of the system output (controlled variable, CV) and its setpoint is integrated, and the integral value is fed to the input of the process (the so-called manipulated variable, MV), which results in a robust adaptation of the system output to the setpoint (Fig. 1). Recently, El-Samad et al. (15) have shown that calcium homeostasis under hypo-

calcemia conditions can be described on the basis of an integral feedback approach, where the error between the calcium setpoint and the actual calcium level is related to the activity of the parathyroid hormone (PTH), an important hormone in calcium regulation.

However, the molecular mechanisms behind error-sensing processes are little understood. To investigate the relationship between the integral control/feedback concept and its reaction kinetic realization, we provide here a kinetic analysis. We show that robust perfect adaptation (homeostasis) is associated with a control species working under zero-order flux conditions while acting on another control species in the way of a “control of the controller”. There is an interesting and close analogy between the mechanisms shown here and mechanisms found in mammalian iron and calcium homeostasis, indicating that other homeostatic mechanisms may underlie similar control structures.

Computational methods

Rate equations were solved numerically by using the FORTRAN subroutine LSODE (Livermore Solver of Ordinary Differential Equations) (16) and MATLAB (www.mathworks.com). To make notations simpler, concentrations are denoted by their names without square brackets.

RESULTS

Molecular representation of integral control

Fig. 2 *a* shows a simple scheme where a homeostatic-regulated intermediate *A* is being synthesized, transformed, and

Submitted March 29, 2009, and accepted for publication June 18, 2009.

*Correspondence: peter.ruoff@uis.no

Editor: Herbert Levine.

© 2009 by the Biophysical Society
0006-3495/09/09/1244/10 \$2.00

doi: 10.1016/j.bpj.2009.06.030

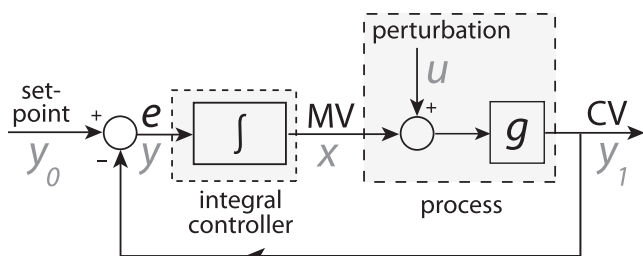


FIGURE 1 Scheme of integral control/feedback of a perturbed system, where the system output is perfectly adapted to the setpoint (i.e., the error e is robustly controlled to zero). MV and CV are the manipulated and controlled variables, respectively. Symbols in gray denote the notation for integral feedback by Yi et al. (14).

degraded. Rate constant k_{pert} indicates an environmental perturbation, such as a sudden increase in A . To avoid possible cell damage by excess of A , A has to be homeostatically regulated. A way to achieve this is to use an A -induced enzyme, E_{adapt} , which clears the cell for excess A . To make the homeostasis perfect, i.e., A adapts always to the same A_{set} value, the rate in the formation of E_{adapt} has to be proportional to the difference (i.e., the error) between A and its setpoint, A_{set} , as indicated by the following equations and shown in Fig. 2, *a* and *b*:

$$\frac{dA}{dt} = k_{\text{synth}} + k_{\text{pert}} - \frac{V_{\text{max}}^{E_{\text{tr}}} A}{K_{\text{M}}^{E_{\text{tr}}} + A} - \frac{V_{\text{max}}^{E_{\text{adapt}}} A}{K_{\text{M}}^{E_{\text{adapt}}} + A}, \quad (1)$$

$$\frac{dE_{\text{adapt}}}{dt} = k_{\text{adapt}}(A - A_{\text{set}}). \quad (2)$$

However, writing the rate of formation of E_{adapt} in proportion to the error $(A - A_{\text{set}})$ (Eqs. 1 and 2, and Fig. 2 *c*) does still lack a molecular understanding of how the setpoint A_{set} is determined. In addition, treating the setpoint A_{set} as a fixed parameter can lead to the problem that, for certain parameter values, concentrations in E_{adapt} may become negative (Fig. 2 *b*).

To avoid negative concentrations, the zero-order term in Eq. 2, $j_0 = k_{\text{adapt}}A_{\text{set}}$, has to be replaced in a kinetically plausible way. A possibility is the removal of E_{adapt} by an additional controller/enzymatic species (E_{set}) working at zero-order conditions. In this case, the set-value A_{set} is then determined by E_{set} 's maximum velocity, $V_{\text{max}}^{E_{\text{set}}}$, divided by the A -induced influx rate, which generates E_{adapt} (Eq. 3). Fig. 3 shows two representations of this mechanism with robust perfect adaptation/homeostasis in A avoiding any negative concentrations. In Fig. 3 *a*, a fully expanded Michaelis-Menten mechanism is shown, whereas in Fig. 3 *b* the mechanism is formulated in terms of steady-state or rapid equilibrium assumptions for the individual enzymatic steps. The kinetic equations with rate constants are given in the Appendix. For both cases, the setpoint in A is given by

$$A_{\text{set}} = \frac{V_{\text{max}}^{E_{\text{set}}}}{k_{\text{adapt}}} = \frac{k_{\text{cat}}^{E_{\text{set}}} E_{\text{set}}^{\text{tot}}}{k_{\text{adapt}}}, \quad (3)$$

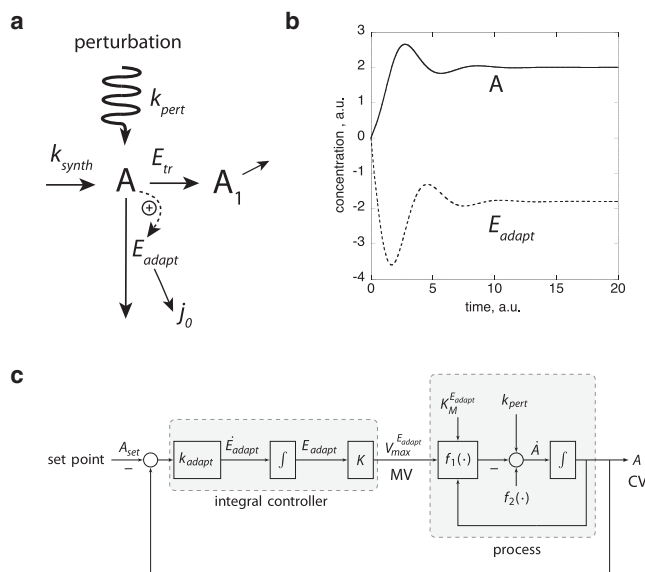


FIGURE 2 (*a*) Reaction scheme of system with rate Eqs. 1 and 2. Species A is formed by a zero-order process with rate constant k_{synth} and then transformed to the product A_1 . Rate constant k_{pert} is related to a perturbing process (wavy line), which increases the level of A . To remove excess A , A is forming enzyme species E_{adapt} , which removes A with the flux $V_{\text{max}}^{E_{\text{adapt}}} A / (K_{\text{M}}^{E_{\text{adapt}}} + A)$ (indicated by the vertical arrow). To get robust adaptation in A independent of k_{pert} , E_{adapt} is removed through a zero-order flux $j_0 = k_{\text{adapt}}A_{\text{set}}$. (*b*) Calculation showing that negative E_{adapt} concentrations may arise when A_{set} is regarded as a fixed setpoint. Initial concentrations of A and E_{adapt} are zero; $k_{\text{adapt}} = 5$, $k_{\text{pert}} = k_{\text{synth}} = 0.5$, $V_{\text{max}}^{E_{\text{adapt}}} = 1$, $K_{\text{M}}^{E_{\text{adapt}}} = 1$, $V_{\text{max}}^{E_{\text{tr}}} = 110$, $K_{\text{M}}^{E_{\text{tr}}} = 100$, and $A_{\text{set}} = 2$. Concentration and timescales are in arbitrary units (a.u.). (*c*) Scheme of the adaptive process shown in panel *a* containing the setpoint A_{set} , the integral controller and the process units. The controlled variable (CV) is A . Eqs. 1 and 2 are written as $dA/dt = f_2(\cdot) - f_1(\cdot) + k_{\text{pert}}$, $dE_{\text{adapt}}/dt = k_{\text{adapt}}(A - A_{\text{set}})$, respectively, with $f_1(\cdot) = V_{\text{max}}^{E_{\text{tr}}} A / (K_{\text{M}}^{E_{\text{tr}}} + A)$, $f_2(\cdot) = k_{\text{synth}} - V_{\text{max}}^{E_{\text{tr}}} A / (K_{\text{M}}^{E_{\text{tr}}} + A)$, and $V_{\text{max}}^{E_{\text{adapt}}} = K \cdot E_{\text{adapt}}$. K is the turnover number for E_{adapt} , i.e., $K = k_{\text{cat}}^{E_{\text{adapt}}}$. MV: manipulated variable.

where $E_{\text{set}}^{\text{tot}}$ is the total concentration of enzyme E_{set} . Keeping A_{set} fixed, the mechanism shows robust homeostasis in A even when rate constants of the three enzymatic pathways (Fig. 3 *a*) are varied by over six orders of magnitude! Fig. 4 shows the A -homeostasis for the scheme shown in Fig. 3 *a*, using several perturbing and initial conditions (for details, see Appendix and Fig. 3 legend). Fig. 4 *a* shows the homeostasis in A when k_{pert} is increased from 0.0 to 1.0 a.u. In Fig. 4 *b*, a large positive excursion in A is observed when k_{pert} is increased from 1.0 to 1×10^3 a.u., which is accompanied by an increased relaxation time in A for reaching A_{set} . Negative excursions in A are observed when k_{pert} is decreased. This is illustrated in Fig. 4 *c* when k_{pert} is decreased from 1.0 to 1×10^{-3} a.u.

However, due to the introduction of enzymatic zero-order kinetics (for avoiding negative concentrations in E_{adapt}), both mechanisms in Fig. 3 show homeostasis only for perturbations, which result in increased or moderate decreased levels in A . When a perturbation removes A too quickly, then the homeostasis in A breaks down. We therefore call this type

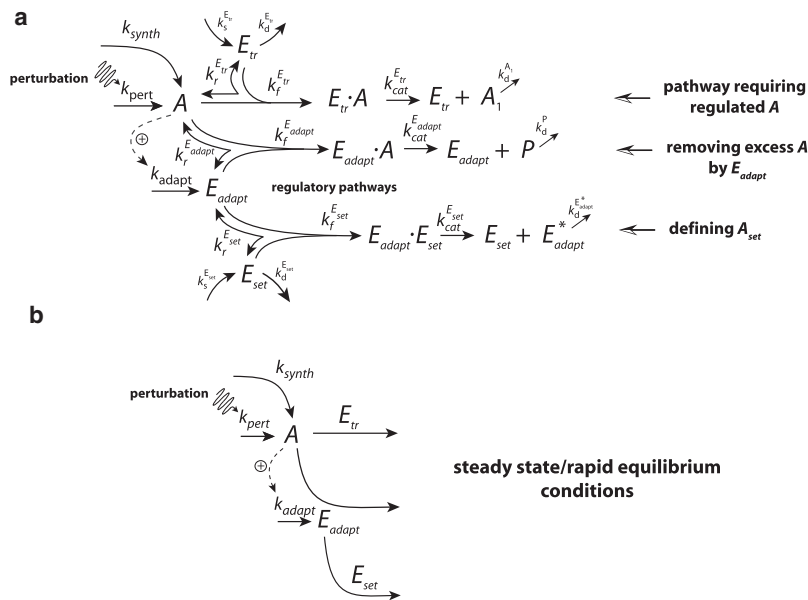


FIGURE 3 To avoid negative concentrations in E_{adapt} , j_0 (Fig. 2 a) is represented as an enzymatic zero-order process. (a) Fully expanded Michaelis-Menten mechanism. The rate equations together with rate constants are shown in the Appendix. To obtain robust homeostasis in A , E_{set} removes active E_{adapt} into an inactive form E_{adapt}^* under zero-order conditions with A_{set} given by Eq. 3. (b) Same mechanism as in panel a, but formulating the Michaelis-Menten mechanism under steady-state/rapid equilibrium conditions. Rate equations are given in the Appendix. A zip-archive containing MATLAB and Berkeley Madonna versions of the model shown in Fig. 3 a with instructions and annotation available in the Supporting Material.

of homeostatic control for inflow-homeostatic control. In Fig. 4 d such a breakdown in A -homeostasis is illustrated by the A steady-state level (A_{ss}) in relation to the (total) concentration of the A -removing enzyme E_{tr} . When the removal rate in A becomes greater than the total production rate ($k_{synth} + k_{pert}$), A_{ss} decreases below A_{set} and homeostasis in A is lost. This type of homeostatic failure can be avoided by using controllers, which specifically address the removal of A (outflow-homeostasis). A mechanism for calcium homeostasis under outflow conditions (hypocalcemia) was recently suggested by El-Samad et al. (15), but in this mechanism, the problem of zero-order fluxes and their association with negative concentrations was not addressed. Specific examples of other inflow and outflow homeostatic mechanisms are discussed below. Fig. 4 e illustrates the breakdown in A -homeostasis when the kinetics in the removal of E_{adapt} by E_{set} is no longer zero-order. For sufficiently large $k_f^{E_{set}}$ values, the $K_M^{E_{set}}$ becomes much lower than E_{adapt} , ensuring zero-order kinetics in the removal of E_{adapt} and leading to A_{ss} values which are equal to A_{set} . For lower $k_f^{E_{set}}$ values, the $K_M^{E_{set}}$ increases and the zero-order kinetics in the removal of E_{adapt} are eventually lost leading to A_{ss} values lower than A_{set} and to the loss in the homeostasis of A . As shown in Fig. 4 e, the A_{ss} values under non-zero-order conditions also depend on k_{pert} . In Fig. 4 f, two A -time profiles are shown for two perturbations, one applied for zero-order conditions ($k_f^{E_{set}} = 10^{12}$, upper curve), and the other for non-zero-order conditions ($k_f^{E_{set}} = 10^6$, lower curve). In both cases, k_{pert} is increased from 1.0 to 5.0 a.u. at $t = 5.0$ a.u. Clearly, zero-order kinetics in the removal of E_{adapt} is required to ensure robust homeostasis in A .

Robust perfect temperature compensation

Temperature is an important environmental parameter, which influences each reaction step in a reaction kinetic

network. Van 't Hoff's rule states that the velocity of a chemical or biochemical process increases generally by a factor between 2 and 3 (the so-called Q_{10}) when the temperature is increased by 10°C . A Q_{10} of 2 corresponds to an activation energy of ~ 50 kJ/mol (17). In general, the concentration of a chemical component, a flux within a kinetic network, or the period length of an oscillatory network, can show temperature compensation/adaptation near a given reference temperature, T_{ref} , when the following balancing equation, here written for the concentration in A , is satisfied (18–21):

$$\frac{d \ln A}{dT} = \frac{1}{RT^2} \sum_i C_{k_i}^A E_i. \quad (4)$$

Here $C_{k_i}^A = \frac{\partial \ln A}{\partial \ln k_i}$ is the control coefficient (22,23) describing how sensitive concentration A is with respect to variations to the network's rate constants k_i . The values R , T , and E_i describe the gas constant, the temperature (in Kelvin), and activation energy (in J/mol) of the process indexed by i , respectively. The balancing equation (Eq. 4) requires a fine-tuning between the control coefficients and activation energies. In general, the resulting temperature compensation in A is not robust, i.e., temperature compensation is only observed within a local region around T_{ref} (see, for example, (24)). Considering the network in Fig. 3, we have 21 rate constants with associated activation energies, and in general, temperature compensation in A is given by Eq. 4 including all 21 terms.

However, this situation changes dramatically when one assumes that E_{adapt} is removed by E_{set} under saturating (zero-order kinetics) conditions and that E_{set} 's turnover is negligible compared to the other fluxes associated with E_{set} . In this case, most of the control coefficients become zero, except for two, which are related to the rate constants k_{adapt} and $k_{cat}^{E_{set}}$. Together with the concentration of E_{set} , k_{adapt}

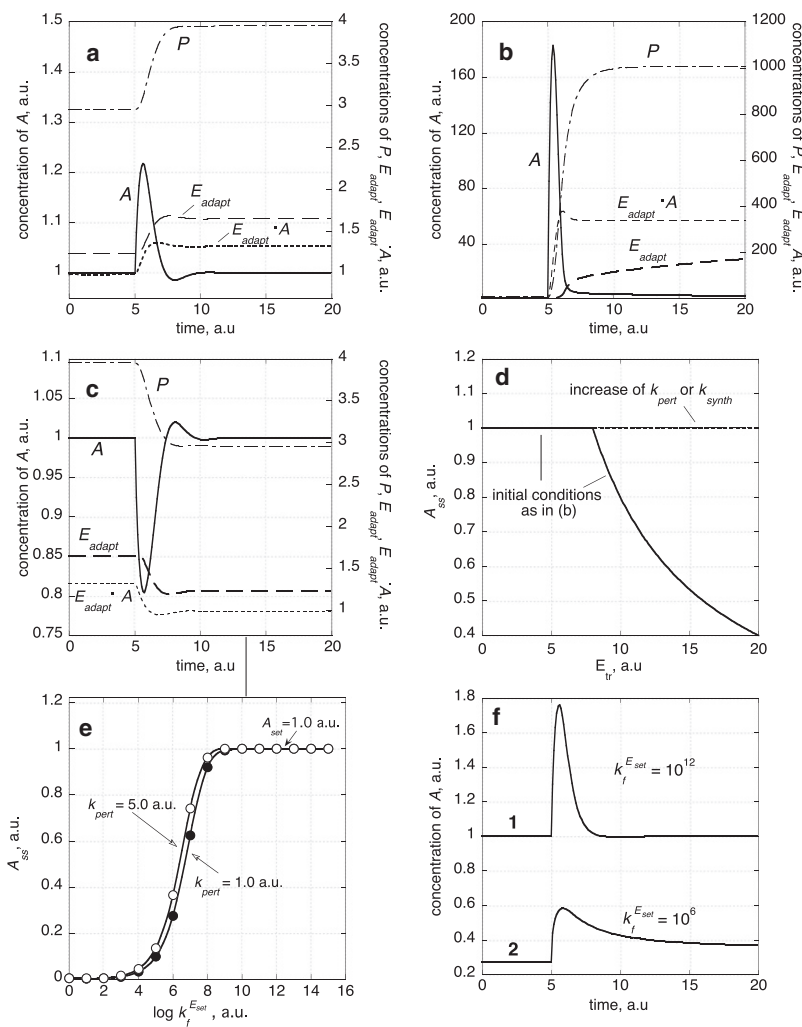


FIGURE 4 Robust perfect adaptation in A with $A_{\text{set}} = 1.0$. (a) Model described in Fig. 3 a with rate constants as given in the Appendix. At $t = 5.0$ time units, k_{pert} is increased from 0.0 to 1.0. (b) Initial conditions as given in the Appendix with $k_{\text{pert}} = 1.0$. At $t = 5.0$ time units, k_{pert} is increased from 1.0 to 10^3 a.u. (c) Initial conditions as in panel b. At $t = 5.0$ time units, k_{pert} is decreased from 1.0 to 10^{-3} a.u. (d) Same initial conditions as in panel b, but E_{tr} is successively increased leading eventually to the breakdown in homeostasis indicated by the decreasing A_{ss} values. This breakdown can be opposed to a certain degree by increasing the values of k_{pert} or k_{synth} . In the figure, k_{pert} or k_{synth} were increased from their original values 1.0 and 3.0 to 10.0 and 12.0, respectively, thereby extending the homeostasis to larger E_{tr} values (dashed line). However, at higher E_{tr} concentrations the homeostasis fails again with decreasing A_{ss} values (data not shown). (e) Calculated A_{ss} values for varying $\log k_f^{E_{\text{set}}}$ with $k_{\text{synth}} = 3.0$ a.u. and $k_{\text{pert}} = 1.0$ a.u. (solid circles), or with $k_{\text{synth}} = 3.0$ a.u. and $k_{\text{pert}} = 5.0$ a.u. (open circles). For $k_f^{E_{\text{set}}} < 10^9$ a.u., perfect homeostasis in A is lost (indicated by the condition that $A_{\text{ss}} < A_{\text{set}}$), because for decreasing $k_f^{E_{\text{set}}}$ the $K_M^{E_{\text{set}}} = (k_{\text{cat}}^{E_{\text{set}}} + k_r^{E_{\text{set}}})/k_f^{E_{\text{set}}}$ associated with the removal of E_{adapt} by E_{set} increases, which eventually leads to the loss of the zero-order kinetics in the E_{adapt} degradation. (f) Time profiles in A with two different $k_f^{E_{\text{set}}}$ values. At $t = 5.0$ time units, k_{pert} is increased from 1.0 to 5.0 a.u. 1 = Perfect homeostasis in A for $k_f^{E_{\text{set}}} = 10^{12}$ a.u.; 2 = Loss of perfect homeostasis in A when $k_f^{E_{\text{set}}} = 10^6$ a.u., which is due to the loss of zero-order kinetics in the degradation of E_{adapt} .

and $k_{\text{cat}}^{E_{\text{set}}}$ define the setpoint for A (Eq. 3). Due to the concentration summation theorem (22,25,26),

$$\sum_i C_{k_i}^A = 0. \quad (5)$$

$C_{k_{\text{adapt}}}^A$ and $C_{k_{\text{cat}}^{E_{\text{set}}}}^A$ have the same magnitude but opposite signs. This indicates that the network can show robust temperature compensation in the level of A when the activation energies for k_{adapt} and $k_{\text{cat}}^{E_{\text{set}}}$ are equal. In fact, when all activation energies are equal, say each reaction step has an activation energy E_a , then all concentrations of the reaction intermediates in the network, I_j , become robust perfectly adapted, as seen by Eq. 6:

$$\frac{d \ln I_j}{dT} = \frac{1}{RT^2} \sum_i C_{k_i}^{I_j} E_a = \frac{E_a}{RT^2} \sum_i C_{k_i}^{I_j} = 0. \quad (6)$$

Fig. 5, a and b, shows this situation for 5°C and 100°C . When activation energies are different (except for the activation energies of k_{adapt} and $k_{\text{cat}}^{E_{\text{set}}}$), then only A shows robust temperature compensation, whereas the concentrations of the other intermediates are no longer invariant. This is indi-

cated in Fig. 5, c and d, for temperature changes between 5°C and 100°C .

DISCUSSION

Zero-order kinetics, integral feedback, and homeostatic breakdown

Integral feedback (14) or integral control (13) is a concept from control theory assuring that the output (the CV, Fig. 1) of a perturbed process is kept at a certain setpoint by integrating the associated error e such that e approaches zero (Fig. 1).

To keep the level of A homeostatic-regulated by integral control/feedback, the rate of formation of an additional species (E_{adapt}) has to be linked to the error, integrated, and then fed into the production rate of A . Integrated A is subtracted from A_{set} and the error e is recalculated (Fig. 2 c). Essential for this approach is the definition of the error e through Eq. 2, which provides the actual condition that A approaches A_{set} when the system's steady state is reached. Critically in this respect is the kinetic interpretation of the

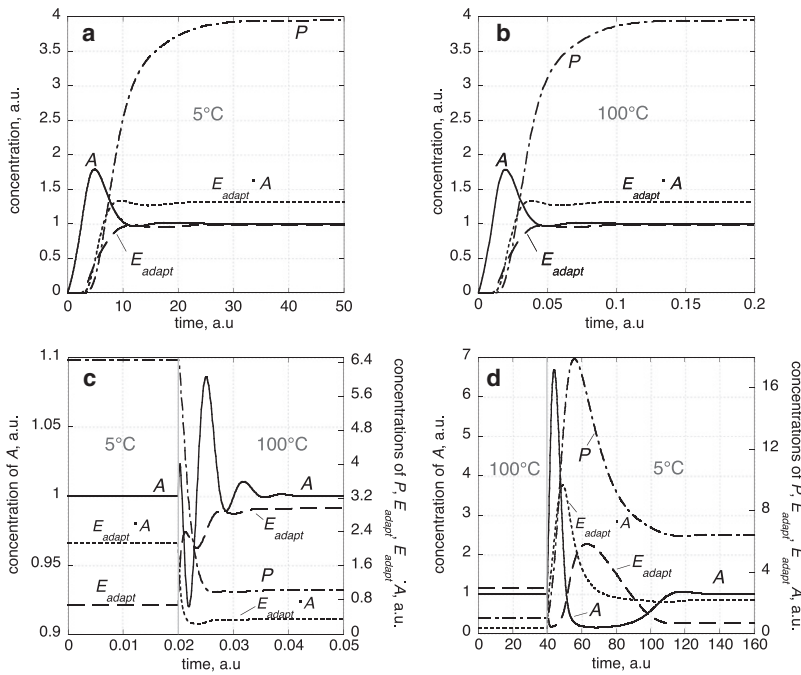


FIGURE 5 Robust perfect temperature compensation of the model described in Fig. 3 *a*. Rate constants (Appendix) refer to 25°C with $A_{\text{set}} = 1$. (a) All activation energies are 50 kJ/mol and temperature is 5°C. (b) All activation energies are 50 kJ/mol and temperature is 100°C. Please note the much shorter timescale compared to panel *a* needed for the system to approach the same steady state. (c) Activation energies are as given in the Appendix. The system is initially at its steady state at 5°C. At 0.02 time units, the temperature is changed to 100°C showing perfect homeostasis only in *A*. (d) Activation energies as in panel *c*. The system is initially at its steady state at 100°C. At 40.0 time units the temperature is changed to 5°C showing perfect homeostasis only in *A*.

term $k_{\text{adapt}}A_{\text{set}}$. To avoid unrealistic situations such as negative concentrations (Fig. 2 *b*), the zero-order flux needs to be put into a proper mechanistic perspective. To achieve this, the mechanism shown in Fig. 3 includes an additional enzymatic species (E_{set}) leading to zero-order degradation/inactivation in E_{adapt} . This step is essential to obtain robust homeostasis. It requires that the level of E_{set} is kept constant and that the ratio between k_{adapt} and $k_{\text{cat}}^{E_{\text{set}}}$ remains unchanged. The latter condition is similar to that found by Levchenko and Iglesias for a model of eukaryotic chemotaxis (27) and a model by Ingalls et al. for a fast excitation-slow inhibition mechanism (Fig. 12.7 in (28)), where activation and inhibition steps are simultaneously activated by a common environmental signal. It may be noted that such a control is, principally, still based on balancing. In our model (Fig. 3 *a*), the balancing between 21 components has been effectively reduced to three parameters, as indicated by Eq. 3.

Interestingly, the kinetic restriction that concentrations must be positive leads to the breakdown of homeostasis for the mechanism in Fig. 3 at high removal/outflow rates in *A*. Whereas the homeostasis in Fig. 2 is robust for both high inflow and high outflow rates in *A* (leading sometimes to unrealistic negative concentrations in E_{adapt}), the chemically realistic mechanism shown in Fig. 3 works only for (high) inflow and moderate outflow rates in *A*. To address the situation of *A*-homeostasis at higher outflow rates (outflow-homeostasis), another homeostatic mechanism is necessary. Fig. 6 shows four motifs of homeostatic control mechanisms, two addressing inflow-homeostasis (Fig. 6, *a* and *b*) and two addressing outflow-homeostasis (Fig. 6, *c* and *d*). Each of these mechanisms work properly when the perturbing inflow and outflow conditions in *A* match their appropriate working conditions, but will fail otherwise, i.e.,

when total outflow in *A* becomes too large for an inflow-homeostatic controller or when total inflow in *A* becomes too large in an outflow-homeostatic controller. Thus, biochemical homeostasis will, in general, require at least two types of mechanisms, i.e., one addressing inflow-homeostasis and another addressing outflow-homeostasis.

Fig. 6 *a* shows an outline of the inflow-control mechanisms described in Fig. 3. The inflow-control mechanism in Fig. 6 *b* shows a related scheme suggested by Yi et al., including a zero order reaction step (14), where instead of the increased removal of *A* the formation of *A* is inhibited by a molecular feedback loop.

Fig. 6 *c* shows an outflow-homeostatic mechanisms closely related to the scheme by El-Samad et al. (15), but avoiding negative concentrations, as shown in their Fig. 8. In our Fig. 6 *d*, outflow homeostatic control is achieved by inhibiting the outflow of *A* through E_{adapt} . In the Appendix we show kinetic representations of these four mechanisms.

Robust perfect adaptation can be related to the concept of integral control or integral feedback (13,14), which involves a negative feedback in the control-theoretic formulation of the system as indicated in Fig. 1 or Fig. 2 *c*. Although some schemes, as in Fig. 6, *b* and *d*, or in the literature (14,29), contain molecular feedback inhibitions (molecular negative feedbacks), the presence of robust perfect adaptation, i.e., the behavior of a control-theoretic negative feedback, does not necessarily require molecular negative feedbacks. An example of robust perfect adaptation with integral feedback behavior but without molecular feedback loops is given by a consecutive reaction such as $\rightarrow A \rightarrow B \rightarrow$, where *B* (or the flux forming *B*) can show robust perfect adaptation for any stepwise change in the rate constant forming intermediate *B* (11,30,31), as long as *A* is formed by zero-order kinetics.

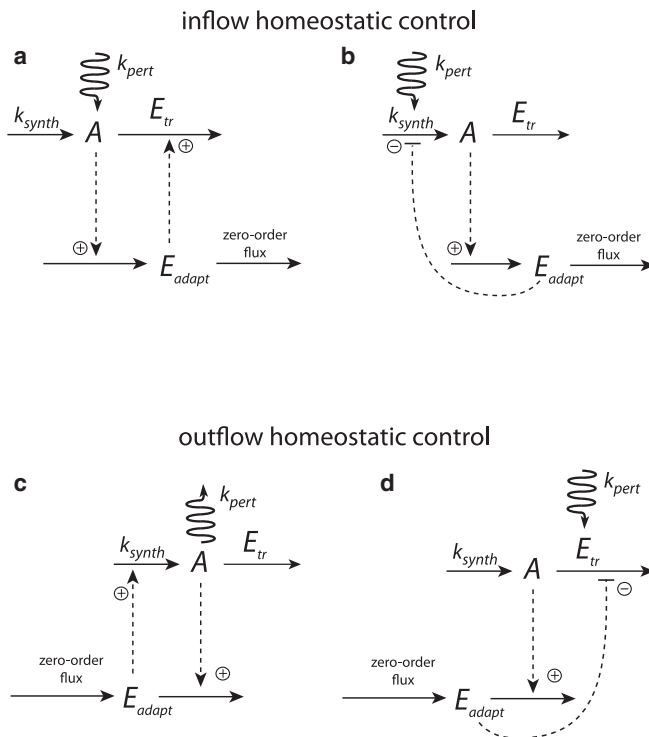


FIGURE 6 Homeostatic control motifs. Due to the kinetic restriction that concentrations need to be positive, two classes of homeostatic controllers arise: 1), inflow homeostatic controllers leading to homeostasis in the concentration of A for increasing (and moderate decreasing) perturbations in A (panels *a* and *b*); and 2), outflow homeostatic controllers leading to homeostasis in A for decreasing (and moderate increasing) perturbations in A (panels *c* and *d*). Rate equations with example parameter values are given in the [Appendix](#). Note that many of the parameter values may be changed within certain limits (besides changing k_{pert}) without affecting the homeostasis. (*a*) Schematic representation of the two (inflow) homeostatic models shown in [Fig. 3](#). Robust homeostasis is due to the zero-order kinetic removal of E_{adapt} . (*b*) Inflow homeostatic model where E_{adapt} inhibits the inflow of A through k_{synth} . To maintain homeostasis the perturbation needs to be applied to the same reaction channel as k_{synth} . The integral feedback is due to the zero-order removal of E_{adapt} and is not related to the physico-chemical negative feedback from E_{adapt} to $(k_{\text{synth}} + k_{\text{pert}})$. (*c*) Outflow homeostatic controller by removing E_{adapt} through A . (*d*) Outflow homeostatic controller by inhibiting E_{tr} through E_{adapt} . Similar to panel *b*, homeostasis is obtained when the perturbation increases the outflow of A through the same reaction channel that is used by enzyme E_{tr} .

Thus, the essential part to get robust homeostasis in the mechanisms shown in [Fig. 6](#), and as illustrated in [Fig. 4, e and f](#), is the presence of the zero-order kinetic term (i.e., “control of the controller”).

Possible regulation points in homeostatic mechanisms

Iron homeostasis

Iron is an essential element for all mammalian cells, but gets toxic when in excess. Special transport and regulatory processes are therefore needed to ensure iron homeostasis within the organism as a whole as well as in individual cells (32). Ferroportin (33) and hepcidin (34) have been suggested to be two key players in iron homeostasis. Ferroportin is an iron exporter, which transports iron from cells such as macrophages or intestinal or liver cells into the blood plasma. Hepcidin, a liver-produced hormone, is a negative regulator of iron absorption with antimicrobial properties, which itself is under homeostatic regulation. An interesting regulatory aspect, which relates to the models in [Fig. 3](#), is that hepcidin binds to ferroportin and leads to its degradation in a similar way as E_{set} removes E_{adapt} . Considering the interaction between ferroportin and hepcidin, the mechanism in [Fig. 3](#) suggests that under iron inflow conditions, hepcidin may serve as a setpoint controller for cell-internal iron concentrations with ferroportin having the role as E_{adapt} , i.e., removing iron (A) out of the cell. The binding between ferroportin (E_{adapt}) and hepcidin (E_{set}), which leads to the degradation of ferroportin (E_{adapt}) (34), may thus provide

a mechanism of how hepcidin acts as a “control of the controller” and leads to potential robust homeostasis. Hepcidin works at concentrations as low as 10 nM (34) and can efficiently reduce upregulated ferroportin levels when iron influx into the cell is high (35). It is not known whether the removal of ferroportin by hepcidin at normal iron concentrations is a zero-order process.

Calcium homeostasis

[Fig. 7](#) shows a scheme of calcium homeostasis in humans. Calcitonin (CT), parathyroid hormone (PTH), and the active form of vitamin D (calcitriol) are important (but not the only) factors involved in the regulation of Ca^{2+} and bone metabolism (36). PTH increases bone resorption and plasma Ca^{2+} levels. Calcitriol increases intestinal Ca^{2+} absorption, bone resorption, and plasma Ca^{2+} . Calcitonin (CT) decreases bone resorption and plasma Ca^{2+} . CaSR denotes the calcium-sensing receptor in the nephron, which appears to mediate effects of hypercalcemia on calcium excretion (37). In case of low calcium levels or when the outflow of calcium needs to be compensated for, an outflow-control mechanism like that indicated in [Fig. 6 c](#) may come into play. The mechanism is similar to that suggested by El-Samad et al. (15) for hypocalcemia. In this mechanism, E_{adapt} plays the role of PTH. The level of PTH is decreased by increased calcium levels. Robust calcium homeostasis is obtained due to a zero kinetic formation rate of E_{adapt} (PTH) and its downregulation by calcium. In the case of high calcium levels, an inflow-control mechanism like that shown in [Fig. 6 a](#) appears to be operative. High calcium (A) levels activate CT and CaSR, which are

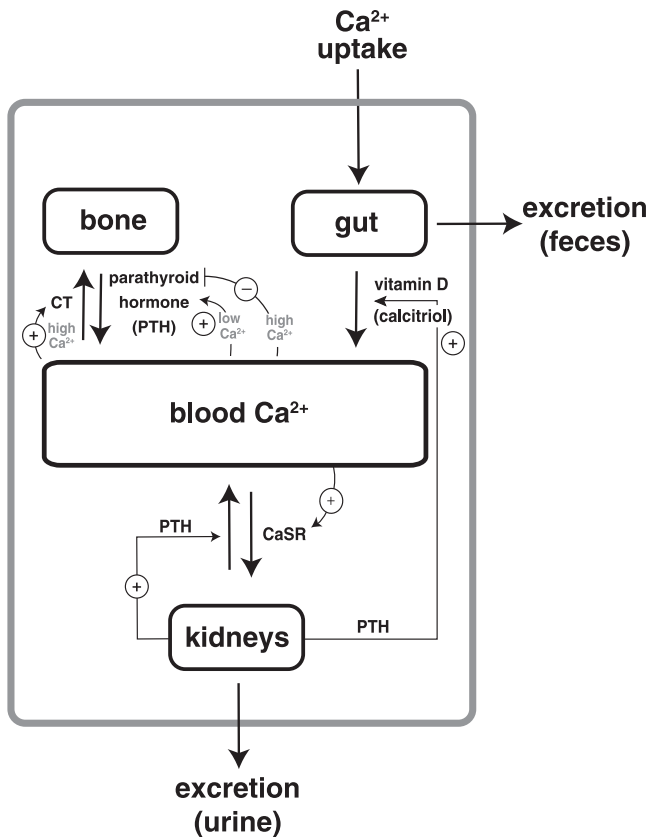


FIGURE 7 Schematic representation of blood calcium homeostasis in humans. Important regulators are parathyroid hormone (PTH), calcitonin (CT), vitamin D, and the calcium-sensing receptor in the nephron. For a discussion of how these regulators may participate in inflow- and outflow mechanisms, see main text.

responsible for the removal of plasma calcium by transporting it into the bone and/or by excretion through the urine. Homeostatic control may be achieved by zero-order kinetic inactivation of CT and/or CaSR.

Robust temperature compensation

It is interesting that the occurrence of robust (activation-energy-independent) temperature compensation for a certain intermediate is closely associated with a robust homeostatic control of that intermediate. This indicates that calcium, iron, and other homeostatic mechanisms may be capable of showing temperature compensation. Unfortunately, there have been few studies in this direction. Herrera et al. (38) studied the temperature dependence of calcium homeostasis in rat pachytene spermatocytes and rat round spermatids in suspension without external calcium concentration. The pachytene spermatocytes showed practically unchanged calcium levels at 10 nmol/L when the temperature was varied (increased) between 16°C and 33°C. Above 33°C, the internal calcium levels quickly increased, reaching levels at 120 nmol/L at 40°C. In the rat round spermatids, the internal calcium levels did not show any temperature compensation,

but a monotonic increase from 30 nmol/L to ~150 nmol/L was observed when the temperature was varied from 5°C to 40°C. Interestingly, the temperature compensation in the calcium homeostasis in the pachytene spermatocytes appears to be due to a balance between two opposing reactions, i.e., between uptake and leakage to and from the cell's internal calcium stores, with determined activation energies of 62 kJ/mol and 55 kJ/mol, respectively.

Although robust homeostatic and adaptation mechanisms appear to be attractive concepts, it is still unclear to what extent temperature compensation (of oscillatory or nonoscillatory processes) is due to a balancing between individual reaction steps (18,21) or due to mechanisms as outlined in Fig. 5, where the balancing is reduced to a few parameters (39). Characteristic to all physiological and chemical temperature compensated systems (20,24,38,40–48) is that the compensation mechanism operates at a local (for the organism) important temperature range and not globally over the whole temperature range such as shown in Fig. 5. However, this does not necessarily invalidate homeostatic control structures as those shown in Figs. 3 and 6. The controllers (for example, E_{adapt} and E_{set}) have to be seen in the context of the dynamics of the whole cell and the whole organism (2), a systems (biology) perspective (49–51), where the controllers themselves are controlled and influenced by factors important for other cellular purposes.

APPENDIX

Rate equations, rate constants, and activation energies for the mechanism in Fig. 3 a.

Rate equations

$$\frac{dA}{dt} = k_{\text{pert}} + k_{\text{synth}} - k_{\text{f}}^{E_{\text{tr}}} A E_{\text{tr}} - k_{\text{f}}^{E_{\text{adapt}}} A E_{\text{adapt}} + k_{\text{r}}^{E_{\text{adapt}}} (E_{\text{adapt}} \cdot A) + k_{\text{r}}^{E_{\text{tr}}} (E_{\text{tr}} \cdot A) \quad (7)$$

$$\frac{dE_{\text{adapt}}}{dt} = k_{\text{adapt}} A - k_{\text{f}}^{E_{\text{adapt}}} A E_{\text{adapt}} + \left(k_{\text{cat}}^{E_{\text{adapt}}} + k_{\text{r}}^{E_{\text{adapt}}} \right) (E_{\text{adapt}} \cdot A) - k_{\text{f}}^{E_{\text{set}}} E_{\text{set}} E_{\text{adapt}} + k_{\text{r}}^{E_{\text{set}}} (E_{\text{adapt}} \cdot E_{\text{set}}), \quad (8)$$

$$\frac{d(E_{\text{adapt}} \cdot A)}{dt} = k_{\text{f}}^{E_{\text{adapt}}} A E_{\text{adapt}} - \left(k_{\text{cat}}^{E_{\text{adapt}}} + k_{\text{r}}^{E_{\text{adapt}}} \right) (E_{\text{adapt}} \cdot A), \quad (9)$$

$$\frac{dP}{dt} = k_{\text{cat}}^{E_{\text{adapt}}} (E_{\text{adapt}} \cdot A) - k_{\text{d}}^{\text{P}} P, \quad (10)$$

$$\frac{dE_{\text{set}}}{dt} = k_{\text{s}}^{E_{\text{set}}} - k_{\text{f}}^{E_{\text{set}}} E_{\text{set}} E_{\text{adapt}} + \left(k_{\text{r}}^{E_{\text{set}}} + k_{\text{cat}}^{E_{\text{set}}} \right) (E_{\text{adapt}} \cdot E_{\text{set}}) - k_{\text{d}}^{E_{\text{set}}} E_{\text{set}}, \quad (11)$$

$$\frac{d(E_{\text{adapt}} \cdot E_{\text{set}})}{dt} = k_f^{E_{\text{set}}} E_{\text{set}} E_{\text{adapt}} - (k_r^{E_{\text{set}}} + k_{\text{cat}}^{E_{\text{set}}}) (E_{\text{adapt}} \cdot E_{\text{set}}), \quad (12)$$

$$\frac{dE_{\text{adapt}}^*}{dt} = k_{\text{cat}}^{E_{\text{set}}} (E_{\text{adapt}} \cdot E_{\text{set}}) - k_d^{E_{\text{set}}} E_{\text{adapt}}^*, \quad (13)$$

$$\frac{dE_{\text{tr}}}{dt} = k_s^{E_{\text{tr}}} - k_d^{E_{\text{tr}}} E_{\text{tr}} - k_f^{E_{\text{tr}}} A E_{\text{tr}} + (k_r^{E_{\text{tr}}} + k_{\text{cat}}^{E_{\text{tr}}}) (E_{\text{tr}} \cdot A), \quad (14)$$

$$\frac{d(E_{\text{tr}} \cdot A)}{dt} = k_f^{E_{\text{tr}}} A E_{\text{tr}} - (k_r^{E_{\text{tr}}} + k_{\text{cat}}^{E_{\text{tr}}}) (E_{\text{tr}} \cdot A), \quad (15)$$

$$\frac{dA_1}{dt} = k_{\text{cat}}^{E_{\text{tr}}} (E_{\text{tr}} \cdot A) - k_d^{A_1} A_1. \quad (16)$$

Rate constants with activation energies

The following rate constants and activation energies (given in parenthesis) have been used unless otherwise stated in the text. Rate constant values refer to 25°C. The Arrhenius equation $k_i = A_i \cdot \exp(-E_i/RT)$ has been used to calculate the rate constant k_i at other temperatures (A_i ; preexponential factor, assumed to be temperature-independent; E_i , activation energy; R , gas constant; and T , temperature in Kelvin). All rate constants are given in arbitrary units (a.u.):

$$\begin{aligned} k_{\text{pert}} &\geq 0 \text{ (70 kJ/mol);} \\ k_f^{E_{\text{adapt}}} &= 4.0 \text{ (50 kJ/mol);} \\ k_r^{E_{\text{adapt}}} &= 2.0 \text{ (40 kJ/mol);} \\ k_{\text{cat}}^{E_{\text{adapt}}} &= 3.0 \text{ (80 kJ/mol);} \\ k_{\text{adapt}} &= 3.0 \text{ (90 kJ/mol);} \\ k_d^P &= 1.0 \text{ (80 kJ/mol);} \\ k_s^{E_{\text{set}}} &= 1.0e - 13 \text{ (70 kJ/mol);} \\ k_d^{E_{\text{set}}} &= 1.0e - 7 \text{ (50 kJ/mol);} \\ k_f^{E_{\text{set}}} &= 1.0e + 11 \text{ (70 kJ/mol);} \\ k_r^{E_{\text{set}}} &= 1.0e + 7 \text{ (60 kJ/mol);} \\ k_{\text{cat}}^{E_{\text{set}}} &= 6.0e + 6 \text{ (90 kJ/mol);} \\ k_d^{E_{\text{adapt}}^*} &= 1.0 \text{ (30 kJ/mol);} \\ k_{\text{synth}} &= 3.0 \text{ (40 kJ/mol);} \\ k_f^{E_{\text{tr}}} &= 1.0 \text{ (50 kJ/mol);} \\ k_r^{E_{\text{tr}}} &= 5.0 \text{ (60 kJ/mol);} \end{aligned}$$

$$k_{\text{cat}}^{E_{\text{tr}}} = 5.0 \text{ (50 kJ/mol);}$$

$$k_d^{A_1} = 1.0 \text{ (40 kJ/mol);}$$

$$k_s^{E_{\text{tr}}} = 1.0 \text{ (50 kJ/mol);}$$

$$k_d^{E_{\text{tr}}} = 10.0 \text{ (70 kJ/mol).}$$

Rate equations for the mechanism in Fig. 3 b/ Fig. 6 a

$$\frac{dA}{dt} = k_{\text{pert}} + k_{\text{synth}} - \frac{V_{\text{max}}^{E_{\text{adapt}}} A}{K_M^{E_{\text{adapt}}} + A} - \frac{V_{\text{max}}^{E_{\text{tr}}} A}{K_M^{E_{\text{tr}}} + A}, \quad (17)$$

$$\frac{dE_{\text{adapt}}}{dt} = k_{\text{adapt}} A - \frac{V_{\text{max}}^{E_{\text{set}}} E_{\text{adapt}}}{K_M^{E_{\text{set}}} + E_{\text{adapt}}}. \quad (18)$$

The following rate constants and initial concentrations give perfect homeostasis with $A_{\text{set}} = 1.0$, $k_{\text{synth}} = 1.0$, and $k_{\text{pert}} \geq 0$: $k_{\text{cat}}^{E_{\text{adapt}}} = 1.0$; $K_M^{E_{\text{adapt}}} = 2.0$; $k_{\text{adapt}} = 3.0$; $k_{\text{cat}}^{E_{\text{set}}} = 6.0e+6$; $K_M^{E_{\text{set}}} = 1.0e-6$; $k_{\text{cat}}^{E_{\text{tr}}} = 0.01$; and $K_M^{E_{\text{tr}}} = 5.0$, where $V_{\text{max}}^{E_{\text{adapt}}} = k_{\text{cat}}^{E_{\text{adapt}}} \cdot E_{\text{adapt}}^{\text{tot}}$; $V_{\text{max}}^{E_{\text{tr}}} = k_{\text{cat}}^{E_{\text{tr}}} \cdot E_{\text{tr}}^{\text{tot}}$; and $V_{\text{max}}^{E_{\text{set}}} = k_{\text{cat}}^{E_{\text{set}}} \cdot E_{\text{set}}^{\text{tot}}$.

Initial concentrations: $A = 1.0$; $E_{\text{adapt}} = 0.01$; $E_{\text{set}}^{\text{tot}} = 5.0e-7$; and $E_{\text{tr}}^{\text{tot}} = 0.1$. Concentrations of $E_{\text{tr}}^{\text{tot}}$ and $E_{\text{set}}^{\text{tot}}$ are kept constant.

Rate equations for the mechanism in Fig. 6 b

$$\frac{dA}{dt} = \frac{(k_{\text{synth}} + k_{\text{pert}})}{(K_I^{E_{\text{adapt}}} + E_{\text{adapt}})} - \frac{V_{\text{max}}^{E_{\text{tr}}} A}{(K_M^{E_{\text{tr}}} + A)}, \quad (19)$$

$$\frac{dE_{\text{adapt}}}{dt} = k_{\text{adapt}} A - \frac{V_{\text{max}}^{E_{\text{set}}} E_{\text{adapt}}}{(K_M^{E_{\text{set}}} + E_{\text{adapt}})}. \quad (20)$$

The following rate constants with zero initial concentrations (both a.u.) give perfect homeostasis in A with $A_{\text{set}} = 1.0$, when varying $k_{\text{pert}} (\geq 0)$: $k_{\text{synth}} = 10.0$; $K_I^{E_{\text{adapt}}} = 0.1$; $V_{\text{max}}^{E_{\text{tr}}} = 40$; $K_M^{E_{\text{tr}}} = 1.0$; $k_{\text{adapt}} = 1.0$; $V_{\text{max}}^{E_{\text{set}}} = 1.0$; and $K_M^{E_{\text{set}}} = 1.0e-6$.

Rate equations for the mechanism in Fig. 6 c

$$\frac{dA}{dt} = k_{\text{synth}} + k E_{\text{adapt}} - k_{\text{pert}} A - \frac{V_{\text{max}}^{E_{\text{tr}}} A}{(K_M^{E_{\text{tr}}} + A)}, \quad (21)$$

$$\frac{dE_{\text{adapt}}}{dt} = j_0 - \frac{V_{\text{max}}^{E_{\text{set}}} E_{\text{adapt}} A}{(K_M^{E_{\text{set}}} + E_{\text{adapt}})}. \quad (22)$$

The following rate constants with zero initial concentrations (both a.u.) give perfect homeostasis in A with $A_{\text{set}} = 1.0$ when varying $k_{\text{pert}} (\geq 0.1)$: $k_{\text{synth}} = 1.0$; $k = 1.0$; and $V_{\text{max}}^{E_{\text{tr}}} = 1$; $K_M^{E_{\text{tr}}} = 0.1$; zero-order flux $j_0 = 1.0$; $V_{\text{max}}^{E_{\text{set}}} = 1.0$; and $K_M^{E_{\text{set}}} = 1.0e-6$.

Rate equations for the mechanism in Fig. 6 d

$$\frac{dA}{dt} = k_{\text{synth}} - \frac{(V_{\text{max}}^{E_{\text{tr}}} + k_{\text{pert}}) A}{(K_M^{E_{\text{tr}}} + A) (K_I^{E_{\text{adapt}}} + E_{\text{adapt}})}, \quad (23)$$

$$\frac{dE_{\text{adapt}}}{dt} = j_0 - \frac{V_{\text{max}}^{E_{\text{set}}} E_{\text{adapt}} A}{(K_{\text{M}}^{E_{\text{set}}} + E_{\text{adapt}})} \quad (24)$$

The following rate constants with zero initial concentrations (both a.u.) give perfect homeostasis in A with $A_{\text{set}} = 1.0$ when varying $k_{\text{pert}} (\geq 0)$: $k_{\text{synth}} = 1.0$; $V_{\text{max}}^{E_{\text{tr}}} = 10$; $K_{\text{M}}^{E_{\text{tr}}} = 1.0$; and $K_{\text{I}}^{E_{\text{adapt}}} = 1.0$; zero-order flux $j_0 = 1.0$; $V_{\text{max}}^{E_{\text{set}}} = 1.0$; and $K_{\text{M}}^{E_{\text{set}}} = 1.0e-6$.

SUPPORTING MATERIAL

Supporting Material files are available at [http://www.biophysj.org/biophysj/supplemental/S0006-3495\(09\)01166-7](http://www.biophysj.org/biophysj/supplemental/S0006-3495(09)01166-7).

This research was supported by the Norwegian Research Council under FUGE Systems Biology (SysMO) grant No. 183085/S10.

REFERENCES

- Asthagiri, A. R., and D. A. Lauffenburger. 2000. Bioengineering models of cell signaling. *Annu. Rev. Biomed. Eng.* 2:31–53.
- Carlson, J. M., and J. Doyle. 2002. Complexity and robustness. *Proc. Natl. Acad. Sci. USA* 99 (Suppl 1):2538–2545.
- Stelling, J., U. Sauer, Z. Szallasi, F. J. Doyle, III, and J. Doyle. 2004. Robustness of cellular functions. *Cell* 118:675–685.
- Kitano, H. 2007. Towards a theory of biological robustness. *Mol. Syst. Biol.* 3:1–7.
- Berg, H. C., and P. M. Tedesco. 1975. Transient response to chemotactic stimuli in *Escherichia coli*. *Proc. Natl. Acad. Sci. USA* 72:3235–3239.
- Barkai, N., and S. Leibler. 1997. Robustness in simple biochemical networks. *Nature* 387:913–917.
- Alon, U., M. G. Surette, N. Barkai, and S. Leibler. 1999. Robustness in bacterial chemotaxis. *Nature* 397:168–171.
- Hansen, C. H., R. G. Endres, and N. S. Wingreen. 2008. Chemotaxis in *Escherichia coli*: a molecular model for robust precise adaptation. *PLoS Comput. Biol.* 4:0014–0027.
- Ratliff, F., H. K. Hartline, and W. H. Miller. 1963. Spatial and temporal aspects of retinal inhibitory interaction. *J. Opt. Soc. Am.* 53:110–120.
- Asthagiri, A. R., C. M. Nelson, A. F. Horwitz, and D. A. Lauffenburger. 1999. Quantitative relationship among integrin-ligand binding, adhesion, and signaling via focal adhesion kinase and extracellular signal-regulated kinase 2. *J. Biol. Chem.* 274:27119–27127.
- Hao, N., M. Behar, T. C. Elston, and H. G. Dohlman. 2007. Systems biology analysis of G protein and MAP kinase signaling in yeast. *Oncogene* 26:3254–3266.
- Mettetal, J. T., D. Muzzey, C. Gómez-Urbe, and A. van Oudenaarden. 2008. The frequency dependence of osmo-adaptation in *Saccharomyces cerevisiae*. *Science* 319:482–484.
- Wilkie, J., M. Johnson, and K. Reza. 2002. Control Engineering. An Introductory Course. Palgrave, New York.
- Yi, T. M., Y. Huang, M. I. Simon, and J. Doyle. 2000. Robust perfect adaptation in bacterial chemotaxis through integral feedback control. *Proc. Natl. Acad. Sci. USA* 97:4649–4653.
- El-Samad, H., J. P. Goff, and M. Khammash. 2002. Calcium homeostasis and parturient hypocalcemia: an integral feedback perspective. *J. Theor. Biol.* 214:17–29.
- Radhakrishnan, K., and A. C. Hindmarsh. 1993. Description and Use of LSODE, the Livermore Solver for Ordinary Differential Equations. NASA Reference Publication 1327, Lawrence Livermore National Laboratory Report UCRL-ID-113855. National Aeronautics and Space Administration, Lewis Research Center, Cleveland, OH.
- Ruoff, P., M. Vinsjevik, and L. Rensing. 2000. Temperature compensation in biological oscillators: a challenge for joint experimental and theoretical analysis. *Comments Theor. Biol.* 5:361–382.
- Ruoff, P. 1992. Introducing temperature-compensation in any reaction kinetic oscillator model. *J. Interdiscipl. Cycle Res.* 23:92–99.
- Ruoff, P., M. K. Christensen, J. Wolf, and R. Heinrich. 2003. Temperature dependency and temperature compensation in a model of yeast glycolytic oscillations. *Biophys. Chem.* 106:179–192.
- Ruoff, P., J. J. Loros, and J. C. Dunlap. 2005. The relationship between FRQ-protein stability and temperature compensation in the *Neurospora* circadian clock. *Proc. Natl. Acad. Sci. USA* 102:17681–17686.
- Ruoff, P., M. Zakhartsev, and H. V. Westerhoff. 2007. Temperature compensation through systems biology. *FEBS J.* 274:940–950.
- Heinrich, R., and S. Schuster. 1996. The Regulation of Cellular Systems. Chapman and Hall, New York.
- Fell, D. 1997. Understanding the Control of Metabolism. Portland Press, London and Miami.
- Aase, S. O., and P. Ruoff. 2008. Semi-algebraic optimization of temperature compensation in a general switch-type negative feedback model of circadian clocks. *J. Math. Biol.* 56:279–292.
- Kacser, H., and J. A. Burns. 1979. Molecular democracy: who shares the controls? *Biochem. Soc. Trans.* 7:1149–1160.
- Burns, J. A., A. Cornish-Bowden, A. K. Groen, R. Heinrich, H. Kacser, et al. 1985. Control analysis of metabolic systems. *Trends Biochem. Sci.* 19:16.
- Levchenko, A., and P. A. Iglesias. 2002. Models of eukaryotic gradient sensing: application to chemotaxis of amoebae and neutrophils. *Biophys. J.* 82:50–63.
- Ingalls, B. P., T.-M. Yi, and P. A. Iglesias. 2006. Using control theory to study biology. In System Modeling in Cellular Biology. Z. Szallasi, J. Stelling, and V. Periwál, editors. MIT Press, Cambridge, MA.
- Alon, U. 2006. An Introduction to Systems Biology: Design Principles of Biological Circuits. Chapman & Hall, New York.
- Csikasz-Nagy, A., and O. S. Soyer. 2008. Adaptive dynamics with a single two-state protein. *J.R. Soc. Interface* 5 (Suppl 1):S41–S47.
- Drengstig, T., H. R. Ueda, and P. Ruoff. 2008. Predicting perfect adaptation motifs in reaction kinetic networks. *J. Phys. Chem. B.* 112:16752–16758.
- Andrews, N. C., and P. J. Schmidt. 2007. Iron homeostasis. *Annu. Rev. Physiol.* 69:69–85.
- Donovan, A., C. A. Lima, J. L. Pinkus, G. S. Pinkus, L. I. Zon, et al. 2005. The iron exporter ferroportin/Slc40a1 is essential for iron homeostasis. *Cell Metab.* 1:191–200.
- Nemeth, E., M. S. Tuttle, J. Powelson, M. B. Vaughn, A. Donovan, et al. 2004. Hepcidin regulates cellular iron efflux by binding to ferroportin and inducing its internalization. *Science* 306:2090–2093.
- Delaby, C., N. Pilard, A. S. Goncalves, C. Beaumont, and F. Canonner-Hergaux. 2005. Presence of the iron exporter ferroportin at the plasma membrane of macrophages is enhanced by iron loading and down-regulated by hepcidin. *Blood* 106:3979–3984.
- Molina, P. E. 2006. Endocrine Physiology. McGraw-Hill, Blacklick, OH.
- Friedman, P. A. 1999. Calcium transport in the kidney. *Curr. Opin. Nephrol. Hypertens.* 8:589–595.
- Herrera, E., K. Salas, N. Lagos, D. J. Benos, and J. G. Reyes. 2001. Temperature dependence of intracellular Ca^{2+} homeostasis in rat meiotic and postmeiotic spermatogenic cells. *Reproduction* 122:545–551.
- Hong, C. I., E. D. Conrad, and J. J. Tyson. 2007. A proposal for robust temperature compensation of circadian rhythms. *Proc. Natl. Acad. Sci. USA* 104:1195–1200.
- Hastings, J. W., and B. M. Sweeney. 1957. On the mechanism of temperature independence in a biological clock. *Proc. Natl. Acad. Sci. USA* 43:804–811.
- Bünning, E. 1963. The Physiological Clock. Springer-Verlag, Berlin.

42. Zimmerman, W. F., C. S. Pittendrigh, and T. Pavlidis. 1968. Temperature compensation of the circadian oscillation in *Drosophila pseudoobscura* and its entrainment by temperature cycles. *J. Insect Physiol.* 14:669–684.
43. Hazel, J. R., and C. L. Prosser. 1974. Molecular mechanisms of temperature compensation in poikilotherms. *Physiol. Rev.* 54:620–677.
44. Aronson, B. D., K. A. Johnson, and J. C. Dunlap. 1994. Circadian clock locus frequency: protein encoded by a single open reading frame defines period length and temperature compensation. *Proc. Natl. Acad. Sci. USA.* 91:7683–7687.
45. Rábai, G., and I. Hanazaki. 1999. Temperature compensation in the oscillatory hydrogen peroxide-thiosulfate-sulfite flow system. *Chem. Comm.* 19:1965–1966.
46. Kóvacs, K. M., and G. Rábai. 2002. Temperature-compensation in pH-oscillators. *Phys. Chem. Chem. Phys.* 4:5265–5269.
47. Edwards, K. D., J. R. Lynn, P. Gyula, F. Nagy, and A. J. Millar. 2005. Natural allelic variation in the temperature-compensation mechanisms of the *Arabidopsis thaliana* circadian clock. *Genetics.* 170:387–400.
48. Gould, P. D., J. C. Locke, C. Larue, M. Southern, S. J. Davis, et al. 2006. The molecular basis of temperature compensation in the *Arabidopsis* circadian clock. *Plant Cell.* 18:1177–1187.
49. von Bertalanffy, L. 1975. *Perspectives on General System Theory.* George Braziller, New York.
50. Sontag, E. D. 2004. Some new directions in control theory inspired by systems biology. *Syst. Biol. (Stevenage).* 1:9–18.
51. Wolkenhauer, O., S. N. Sreenath, P. Wellstead, M. Ullah, and K. H. Cho. 2005. A systems- and signal-oriented approach to intracellular dynamics. *Biochem. Soc. Trans.* 33:507–515.